Light and Microwaves in Laser Frequency Combs: An Interplay of Spatiotemporal Phenomena

Marco Piccardo, Dmitry Kazakov, Benedikt Schwarz, Paul Chevalier, Arman Amirzhan, Johannes Hillbrand, Sultan Z. AlMutairi, Yongrui Wang, Feng Xie, *Member, IEEE*, Kevin Lascola, Steffen Becker, Lars Hildebrandt, Robert Weih, Alexey Belyanin, and Federico Capasso, *Life Fellow, IEEE*

(Invited Paper)

***Abstract*—Interference of laser beams in a suitable medium creates dynamic optical gratings, which can serve for a wide variety of applications, ranging from real-time holography to ultrasound generation. Typically, the interference occurs in a sample material that is separated from the laser sources. Here, we explore a new aspect of laser-induced dynamic gratings: microwave generation occurring inside the cavity of semiconductor laser frequency comb generators, such as quantum cascade lasers and interband cascade lasers. The interplay between laser light and microwaves in these devices reveals intracavity spatiotemporal phenomena that are of great importance for the understanding of their physics and for their operation to be efficient. Grating effects related to laser locking dynamics, structured cavities, and microwave propagation are demonstrated. Applications in science and technology based on these phenomena, including the realization of novel hybrid electronic–photonic devices, will also be presented.**

***Index Terms*—Dynamic gratings, optical frequency combs, microwave generation, semiconductor lasers, electronic-photonic devices.**

Manuscript received February 13, 2019; revised March 19, 2019; accepted March 22, 2019. Date of publication April 1, 2019; date of current version May 7, 2019. This work was supported by the National Science Foundation Awards No. CCSS-1807323 and ECCS-1614631. This work was performed in part at the Center for Nanoscale Systems, a member of the National Nanotechnology Coordinated Infrastructure Network, which was supported by the National Science Foundation under NSF Award 1541959. The work of B. Schwarz and J. Hillbrand was supported by Austrian Science Fund (FWF) within the projects NanoPlas (P28914N27) and Building Solids for Function (W1243). *(Corresponding\penalty -\@M author: Marco Piccardo.)*

M. Piccardo, D. Kazakov, P. Chevalier, A. Amirzhan, and F. Capasso are with the Harvard John A. Paulson School of Engineering and Applied Sciences, Harvard University, Cambridge, MA 02138 USA (e-mail: piccardo@g.harvard.edu; kazakov@g.harvard.edu; chevalier@g.harvard.edu; amirzhan@g.harvard.edu; capasso@seas.harvard.edu).

B. Schwarz and J. Hillbrand are with the Institute of Solid State Electronics, TU Wien, A-1040 Vienna, Austria (e-mail: benedikt.schwarz@tuwien.ac.at; johannes.hillbrand@tuwien.ac.at).

S. Z. AlMutairi, Y. Wang, and A. Belyanin are with the Department of Physics and Astronomy, Texas A&M University, College Station, TX 77843 USA (e-mail: szalmutairi@tamu.edu; wangyongrui@physics.tamu.edu; belyanin@physics.tamu.edu).

F. Xie and K. Lascola are with Thorlabs Quantum Electronics, Jessup, MD 20794 USA (e-mail: fxie@thorlabs.com; klascola@thorlabs.com).

S. Becker, L. Hildebrandt, and R. Weih are with the nanoplus Nanosystems and Technologies GmbH, 97218 Gerbrunn, Germany (e-mail: steffen.becker@nanoplus.com; lars.hildebrandt@nanoplus.com; robert.weih@nanoplus.com).

Color versions of one or more of the figures in this paper are available online at http://ieeexplore.ieee.org.

Digital Object Identifier 10.1109/JSTQE.2019.2908553

I. Introduction

INTERFERENCE of two light beams creates a spatially periodic intensity distribution [1]. By placing a suitable material in the interference region, one can observe the intensity wave spatially modulating the optical properties of the medium, such as the refractive index and absorption coefficient, inducing an optical grating structure. Such type of gratings can be used in applications like real-time holography [2], optical logic [3], and beam deflection and modulation in photonic devices [4]. Moreover, due to the nonlinearity of the light-matter interaction, the interfering light beams can generate new waves, e.g., ultrasounds [5], with a different direction and frequency. In this work we report on a new aspect of optical gratings: microwave generation in semiconductor lasers, and related applications in science and technology.

The formation of a laser-induced grating can be understood as follows. Consider two light beams with the same polarization, same wavelength λ, and propagation vectors $\vec{k}_1$ and $\vec{k}_2$ intercepting at an angle θ (Fig. 1a). The interference region will be modulated with a grating vector $q = \pm(\vec{k}_1 - \vec{k}_2)$, where the sign ambiguity is due to the fact that the grating is stationary (this is represented by a double-headed arrow in Fig. 1). The lateral extension of the grating is limited by the finite cross section of the beams. The period of the intensity pattern is $\lambda/(2\sin\theta/2)$, thus it can be tuned simply by varying the interception angle of the beams. In the limit of $\theta = \pi$ corresponding to counter-propagating waves, the familiar case of a standing wave in a cavity with period $\lambda/2$ is obtained (Fig. 1b). When such intensity pattern occurs inside an optical medium, it induces a stratification of the material, forming in essence a volume hologram that is also known as a Lippman grating. If instead one considers two co-propagating waves with different frequencies ω_1 and ω_2, a moving grating is produced (Fig. 1c), with wave vector $\vec{q} = \vec{k}_1 - \vec{k}_2$ characterized by a well-defined propagation direction (note the single-headed arrow in Fig. 1) and frequency given by $\omega_1 - \omega_2$. Finally, a third type of dynamic grating is generated when both counter-propagating waves at the same frequency and co-propagating waves at different frequencies interfere. In the most elementary example of this kind, four waves interfere ($\vec{k}_1$, $\vec{k}_2$, $\vec{k}_3$, $\vec{k}_4$) giving six interference products (Fig. 1d): two of these are stationary gratings ($q_{1,2}$, $q_{3,4}$), while the others

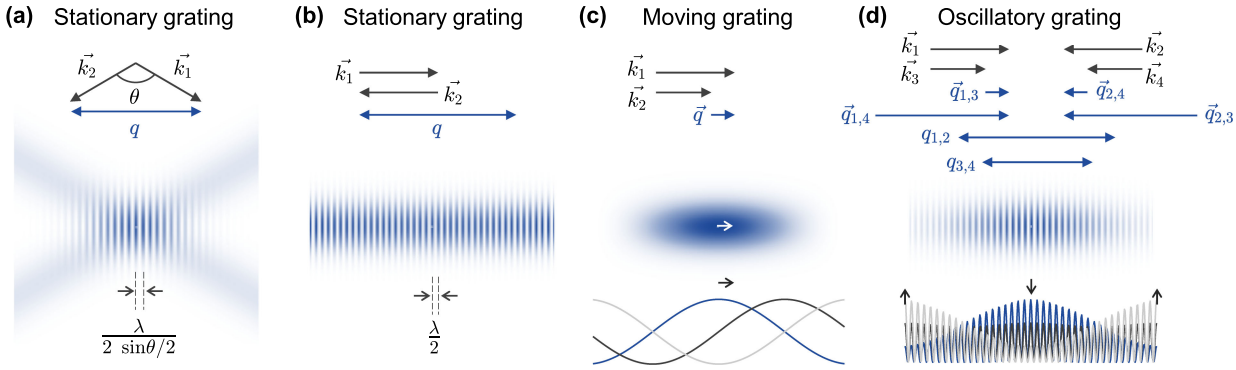

Fig. 1. Different types of optical gratings created by beam interference in a medium. (a) Stationary grating produced by two beams with the same wavelength λ intercepting at an angle θ. The plot represents the intensity of the waves. (b) Stationary grating generated by two counter-propagating waves with the same wavelength. (c) Moving grating created by two co-propagating waves with different wavelengths. The grating moves in the direction of the grating wave vector $\vec{q}$. Also shown are cuts of the grating pattern along the propagation direction taken at different times: $t = 0$ (blue), $t = T_B/4$ (black), $t = T_B/2$ (grey), T_B being the beat period of the waves. (d) Oscillatory grating produced by the interference of four waves: $\vec{k}_1 = -\vec{k}_2$, $\vec{k}_3 = -\vec{k}_4$. The grating oscillates in amplitude but does not propagate in space. Also shown are cuts of the grating pattern along the direction of the wave vectors taken at different times: $t = 0$ (blue), $t = T_B/4$ (black) and $t = T_B/2$ (grey).

produce two oscillatory gratings with a short ($\vec{q}_{1,3}$, $\vec{q}_{2,4}$) and a long ($\vec{q}_{1,4}$, $\vec{q}_{2,3}$) wave vector, which oscillate in amplitude at the beat frequency ($\omega_1 - \omega_3 = \omega_2 - \omega_4$) but do not propagate in space.

The vast majority of optical gratings applications are based on lasers, as these are ideal light sources to produce strong interference patterns, thanks to their coherence, collimation and high intensity. We restrain ourselves in the following to mention only few recent examples of uses of laser-induced dynamic gratings. Xiong *et al.* intercepted two beams at different frequencies in a photoacoustic cell to create a moving grating [6]. By tuning the interception angle, they achieved a resonance condition for which the optical grating moves at the same speed of the sound wave generated by the photoacoustic effect. This enabled a highly sensitive trace gas detector. Yang *et al.* employed two non-collinear beams with orthogonal polarization to create a standing wave of photon helicity in a two-dimensional electron gas, inducing a spin density wave [7]. This produces variations in the refractive index acting as a transient grating which can be monitored by the diffraction of a third beam, giving information on the spin propagation dynamics, which is essential for the development of spin-based electronics. Odoulov *et al.* showed that intercepting in a medium two beams of different colours, such as blue and green, allows one to record holograms even when the moving grating travels almost at the speed of light [8]. This was a surprising result as one would expect that the medium cannot follow the fringe displacement due to its limited slow response time. The key for this result was to use short laser pulses giving a very short exposure time which may be used in ultrafast nonlinear spectroscopy. While the examples given above describe cases where the optical grating is produced in a sample material, there have also been studies of intrinsic dynamic gratings occurring inside the laser source itself. For instance, Peterka *et al.* investigated the dynamics of self-swept fiber lasers [9]. Due to spatial hole burning in the fiber, the laser hops regularly from one longitudinal mode to the next one inducing at each hop a new refractive index grating with a different pitch. Bardella *et al.* studied the role of carrier gratings induced by the optical standing waves in quantum dot lasers showing that this is responsible for multimode operation of these devices [10]. A notable effect there was that the carrier grating is not washed out by diffusion like in quantum well lasers, thanks to carrier trapping in the quantum boxes.

As shown by the previous examples, stationary and moving gratings have been widely exploited and studied in the literature, however oscillatory gratings are still relatively unexplored. This work focuses on this type of optical gratings. In particular, we study their occurrence in multimode semiconductor lasers which can act as transducers converting the optical oscillations into microwaves. This gives new insights into the physics of this class of lasers and endows them with novel functionalities.

II. Light Generating Microwaves

A. Mechanism

Consider a semiconductor laser with a Fabry-Perot geometry, so that cavity modes are standing waves. In such a laser, the first mode oscillating inside the cavity induces a stationary grating of population inversion (as in Fig. 1b), provided that the carrier diffusion length is smaller than the grating period. Due to this phenomenon, known as spatial hole burning, other longitudinal modes can extract gain from the medium and start lasing, resulting in multi-wavelength emission. This type of laser then contains all the elements to produce oscillatory gratings, since both counter-propagating waves and waves at different frequencies exist (cf. Fig. 2a and Fig. 1d). The spatiotemporal variations of optical intensity inside the cavity create by means of stimulated emission and absorption time-dependent population inversion gratings in the gain medium [11]. This generates a radio frequency voltage across the active region of the laser – typically oscillating at frequencies in the gigahertz range for millimeter-long cavities – giving origin to microwaves.

In presence of dispersion, the Fabry-Perot cavity modes have wave vectors that are regularly spaced, given by $k_m = \pi m/L$

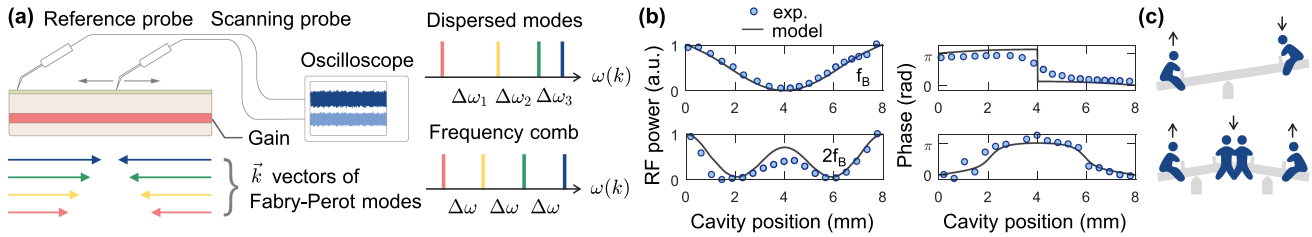

Fig. 2. Measurement of microwave gratings in semiconductor lasers. (a) A Fabry-Perot laser contains all the elements to generate oscillatory gratings thanks to the presence of counter-propagating waves with different frequencies. Microwaves are generated at the beat frequencies of the optical modes, which are narrow tones when the laser operates in the optical frequency comb regime, thanks to its uniform spacing. A near-field scanning probe technique allows to measure these oscillatory gratings arising in the gain medium. Two microwave probes are used in order to extract the beating signal, which is analyzed in the time-domain using an oscilloscope. (b) Example of microwave gratings measured in a quantum cascade laser. Both the measured amplitude and phase are plotted for gratings oscillating at the fundamental (f_B) and second-harmonic ($2f_B$) beat note of the laser. These correspond to a periodic motion similar to that of seesaws (c). Also shown in (b) are the predictions of an analytical model based on the interference of standing-waves.

with m being the mode index and L the cavity length, but frequencies that are not equidistant (Fig. 2a), given by $\omega_m = ck_m/n(\omega_m)$ with n being the effective refractive index of the waveguide. This implies that the beating of longitudinal modes can generate oscillatory gratings with the same spatial period (e.g., $q = k_{m+1} - k_m = k_m - k_{m-1}$) but different frequencies (e.g., $\Delta\omega_1 = \omega_{m+1} - \omega_m$, $\Delta\omega_2 = \omega_m - \omega_{m-1}$). This in turn causes a spread of the energy of a grating with a given $\vec{q}$ in the frequency domain, making this effect experimentally hard to observe. If instead an efficient locking mechanism is present in the laser, such as four-wave-mixing, multimode operation may lead to the formation of an optical frequency comb, where the modes are equally spaced in frequency (Fig. 2a). Then all gratings with a given $\vec{q}$ oscillate at the same frequency $\Delta\omega$, which permits to add up coherently their energy and enhance the magnitude of the effect, ultimately making it easier to measure.

B. Detection

The measurement of microwave gratings in semiconductor lasers that we implemented relies on a near-field scanning technique. A schematic of the experimental set-up is shown in Fig. 2a. Two microwave probes are placed on the top electrode of the laser: one is scanned along the longitudinal axis of the cavity using a micrometer position stage, while the other one is kept at a fixed position to provide a phase reference. We use signal-only probes (rather than ground-signal or ground-signal-ground probes), as this minimizes outcoupling of the microwave power and helps to avoid perturbing the laser operation. The signal extracted from the probes can be analyzed either in the time domain or in the frequency domain in order to obtain both the amplitude and phase of the gratings. This can be achieved by time-domain reconstruction using a mixed-signal oscilloscope with sufficiently high bandwidth to follow the laser beat notes, or with a low-bandwidth oscilloscope used in conjunction with a down-conversion set-up bringing the laser beat notes in a lower frequency range, e.g., megahertz. A frequency-domain alternative is to use lock-in detection of a possibly downconverted beat-note, should it lie outside of the lock-in detection bandwidth.

This type of measurement is reminiscent of the slotted line technique which was used in microwave systems few decades ago [12], before the appearance of network analyzers. In that case a slot was opened in a microwave transmission line in order to place a probe, which was scanned to measure the voltage-standing-wave-ratio of the microwave. Similarly to our technique, the scanning pickup probe behaved as an antenna measuring the electric field modulation, thus being sensitive to the voltage profile of the microwave.

C. Example of Gratings

Many oscillatory gratings with different spatial and temporal frequencies, are generated in a laser frequency comb. Since the gratings are linearly superposed they can be easily distinguished by Fourier decomposition in the frequency domain. Moreover, they can be divided into two categories based on the typical size of their spatial period: gratings with short $\vec{q}$, which are produced by the difference frequency of the wave vectors of Fabry-Perot modes, and with long $\vec{q}$, which are given by the sum frequency of the wave vectors (Fig. 1d). Up to the present time, only gratings with short $\vec{q}$ could be measured using the technique described above. Long $\vec{q}$ gratings have a spatial period of the order of the optical wavelength, being much smaller than the size of the used microwave probe ($\sim$100 μm), thus should be averaged out in the measurement. (It remains to be determined if long $\vec{q}$ gratings are measurable at all, even using fine-tip probes, as they may be already washed out inside the laser due to microwave in-plane propagation. Such effects will be discussed in Section III-C.)

An example of microwave gratings measured in a quantum cascade laser (QCL) frequency comb [13] is shown in Fig. 2b. The gratings oscillate at the fundamental (top, $f_B = 5.6$ GHz) and second-harmonic (bottom, $2f_B = 11.2$ GHz) beat frequencies of the laser, corresponding to the beating of adjacent modes and second-order neighbors, respectively. Both the power and phase of the gratings are shown. The patterns exhibits antinodes at the edge of the cavity and a number of nodes corresponding to the beat note order. The dynamics of the voltage profiles corresponds to anti-phase oscillations of adjacent lobes, as in the motion of seesaws (Fig. 2c). Also shown in Fig. 2b are the curves predicted by an analytical model, which accounts for the interference effects in the standing-wave cavity, giving a good agreement with the experimental results. According to this

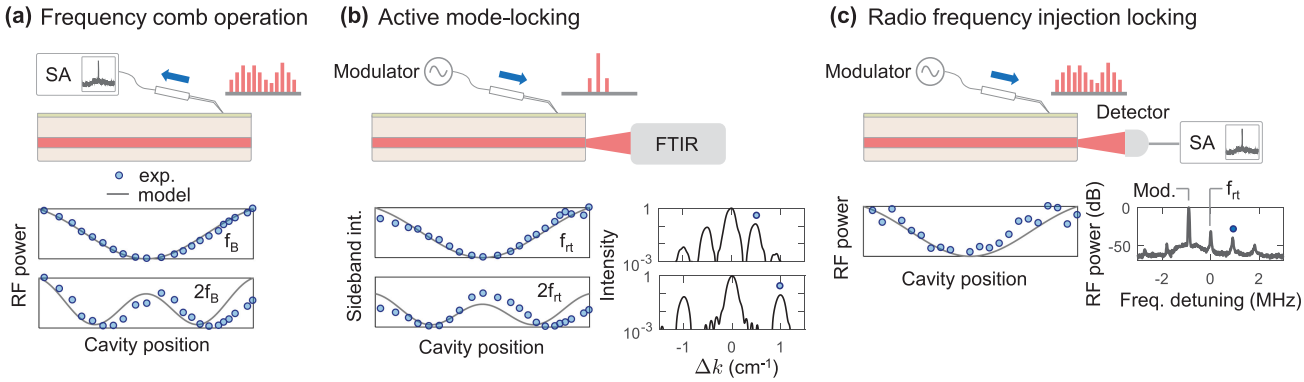

Fig. 3. Occurrence of gratings in laser locking dynamics. (a) Microwave gratings measured at the fundamental (f_B) and second-harmonic ($2f_B$) beat note of a quantum cascade laser operating in the frequency comb regime. The radio frequency (RF) power of the beat notes is detected using a spectrum analyzer (SA). (b) Active mode-locking experiment carried out on the same device as in (a). Here the laser initially operates in the single mode regime, and a radio frequency modulation is applied via a microwave probe at a given position on the top electrode of the laser. This generates optical sidebands separated from the initial lasing mode by the modulation frequency. The sidebands can be observed by measuring the laser output with a Fourier transform infrared spectrometer (FTIR). Two representative optical spectra are shown for modulation frequencies corresponding to the laser roundtrip frequency (f_{rt}, top) and its second harmonic ($2f_{rt}$, bottom). The measurement at f_{rt} was done with 16 dBm at ≈14.9 GHz sourced from the microwave generator and at $2f_{rt}$ with 24 dBm at ≈29.8 GHz. Wave numbers are referenced to that of the central mode ($k = 1343$ cm^{-1}). The intensity of one of the optical sidebands (indicated by a dot in the spectra) is plotted as a function the cavity position where the modulating microwave signal is applied. (c) Radio frequency injection locking experiment carried out on the same device as in (a) and (b). Here the device initially operates in a frequency comb regime with intermodal spacing $f_{\rm rt}$, then a 20 dBm modulating signal at a slightly different frequency (0.9 MHz detuning) is applied using a microwave probe placed on the top electrode of the device. The laser output is measured using a fast detector, whose radio frequency signal is analyzed with a spectrum analyzer (SA). A representative RF spectrum is shown, that features sidebands produced by a frequency pulling effect. The intensity of the strongest RF sideband (marked by a dot) is plotted as a function of the position in the cavity where the modulating microwave probe is placed. Also shown in (a)–(c) are the predictions of the experimentally observed effects of different analytical models described in the text. The device geometry was not optimized for radio frequency performance, limiting the power transfer between the microwave generator and the QCL chip in these experiments.

model [11], the intracavity intensity variation oscillating at the n-th harmonic of the fundamental beat note frequency is given by

$$I_{B,n} = \sum_{m=1}^{N-n} A_m A_{m+n} \Big[\cos\left(nk_B x + n\omega_B t + \Delta\phi_{m+n,m}\right) e^{-gx} + R_1 \cos\left(nk_B x - n\omega_B t - \Delta\phi_{m+n,m}\right) e^{gx} \Big] \quad (1)$$

where N is the number of lasing modes, A_m and A_{m+n} are the amplitudes of mode m and $m+n$, k_B and ω_B are determined by the difference of wave vectors and angular frequencies of any pair of adjacent modes, $\Delta\phi_{m+n,m}$ is the difference of the spectral phases of modes $m+n$ and m, $g = \log[1/(R_1 R_2)]/(2L)$ is the net gain coefficient with L being the cavity length and $R_{1,2}$ the facet reflectivities. Since the oscillating intensity produces an AC current, the beat note power will depend on the square of $I_{B,n}$ (for more details, see the model derivation in Ref. [11]).

III. Spatiotemporal Phenomena

The interplay between light and microwaves arising from the physical processes described above gives origin to novel spatiotemporal phenomena in the laser cavity, which have just started to be explored and are of great practical importance for a complete understanding and efficient operation of laser frequency combs. In the following we present a number of these new effects, which relate to laser locking dynamics, structured cavities and microwave propagation. QCLs will be used as a model system. Other types of lasers susceptible to these phenomena are interband cascade lasers (ICLs), which will be presented in Section IV.

A. Gratings and Laser Locking

Active mode-locking is a technique that allows one to create phase-locked modes in a laser by means of an external modulation of the optical field. In semiconductor lasers it can be realized by adding a radio frequency modulation to the bias voltage of the laser. Here we study the efficiency of active mode-locking when the modulation is applied locally at different positions on the top electrode of a QCL by means of a microwave probe. Initially, the laser operates in the single mode regime and, after the modulation is turned on, optical sidebands are generated around the carrier frequency at a frequency detuning given by the modulation frequency (Fig. 3b).

Sidebands are generated by a polarization term induced by the modulator which has the form [14]

$$p_{\pm1}(t) = \frac{\epsilon}{2L} E_0(t) \int_{L_{mod}} \chi_1(x) u_0(x) u_{\pm1}(x) dx \quad (2)$$

where ϵ is the dielectric permittivity, L is the cavity length, L_{mod} is the modulator length, E_0 is the amplitude of the central mode, χ_1 is the amplitude of the linear susceptibility variations induced by the modulator, and u_0 and $u_{\pm1}$ are the longitudinal eigenmodes of the central mode and sidebands. The modulator polarization term gives a rate of change for the sidebands amplitudes given by [14]

$$\left.\frac{dE_{\pm1}}{dt}\right|_{\rm mod} \propto -i\frac{\omega_{\pm1}}{2\epsilon} p_{\pm1}(t) \quad (3)$$

A thorough analysis would require adding this source term to the coupled-mode equations, together with the loss, gain and pulling contributions, and solve for the sideband amplitudes. Here we simply estimate the efficiency of the modulator

using $p_{\pm 1}^2$, where the square is due to the fact that we deal with sideband intensities. This essentially reduces to evaluating the overlap integral of Eq. 2 for different positions of the modulator in the cavity. The size of the modulator is considered to be given by the diameter of the tip of the microwave probe ($\sim$100 μm), which is much smaller than the cavity length (3 mm) and much larger than the optical wavelength (7.6 μm). Thus the probe acts as a small electro-optic intracavity modulator.

Fig. 3b shows the calculated modulator efficiency together with the measured sideband intensity for different positions of the microwave probe along the cavity. Both the results obtained at a modulation frequency corresponding to the cavity roundtrip (f_{rt}) and its second-harmonic ($2f_{rt}$) are shown. Experiments and calculations exhibit very similar patterns. Most importantly, these are the same type of profiles shown by the microwave gratings that form at f_B and $2f_B$ when the same laser operates in the frequency comb regime (Fig. 3a). This is due to the fact that both the formation of a frequency comb and active mode-locking rely on mode coupling, and such profiles provide a spatial picture of this phenomenon.

Another well-known phenomenon in which internal dynamic gratings play a role is the radio frequency injection locking of the comb repetition rate. In this case the laser initially operates in a multimode frequency comb regime with a well-defined narrow intermodal beatnote. By applying a radio frequency modulation to the bias voltage of the laser, its round trip frequency f_{rt} can be locked – provided that the modulation frequency f_{mod} lies within the locking range of the two oscillators Δf_{lock}. If instead the modulation frequency lies just outside the locking range, i.e., $|f_{rt} - f_{mod}| \gtrsim f_{lock}$, the laser output is modulated at new frequencies [15], [16], which can be revealed by measuring the optical output with a fast photodetector and analyzing its modulation spectrum with an RF spectrum analyzer (Fig. 3c). Such additional frequencies appear as sidebands on the radio frequency spectrum. Their power is given by [17]

$$P_n \approx P_{f_{rt}} \left(\frac{\Delta f_{lock}}{2|f_{rt} - f_{mod}|} \right)^{2n} \tag{4}$$

where n is the sideband index, and $P_{f_{rt}}$ is the power of the laser beat note at f_{rt} taken at the position along the cavity where the modulation is applied.

Fig. 3c shows the power of the strongest sideband produced by the injection locking phenomenon just described as measured for different positions of the modulator probe along the laser cavity. This is observed to spatially vary in the same way as the microwave grating at f_B measured in frequency comb operation (Fig. 3a), as expected from Eq. 4. This result also proves that injection locking has the maximum efficiency when the modulation signal is applied at the edge of the cavity [14].

B. Structured Cavities

A common approximation in laser analysis is to ignore the spatial dependence of the intensity field inside the cavity. Such approximation does not prevent to describe many aspects of laser dynamics, however there are several cases in which it is necessary to take into account the intracavity intensity variation in order to understand laser behavior [18]. One example is structured cavities, i.e., resonators integrating elements such as coatings and gratings that affect the internal propagation of light. Despite the importance of intracavity intensity variation in lasers, there are still no well established techniques to characterize this quantity. In gas lasers it was proposed to exploit Rayleigh scattering to measure the intracavity power [19]. The apparatus used a photomultiplier, which measured the light scattered by the gas in a certain direction. In order for the measurement to be local, it was required to use diaphragms to eliminate all scattered light coming from other positions in the cavity. A somewhat similar approach was used in semiconductor lasers [20], [21], where a stripe window was etched on the top electrode of a laser, allowing to measure light generated by spontaneous emission, which can be linked to the carrier density via the bimolecular recombination rate and ultimately to the intensity. The spatial resolution was achieved either using an objective in conjunction with a slit or an optical fiber. In all cases the reconstruction of the intracavity intensity required a modification of the resonator. In the following we show that microwave gratings provide direct information on intracavity intensity variation also in structured cavities. The advantage of this technique, which we name laser intracavity intensity radiofrequency reconstruction (LIIRR), is that it is non-invasive. The main requirement of LIIRR is multimode operation and the possibility of beat note detection.

First, we study the case of an asymmetric Fabry-Perot cavity with high-reflectivity (HR) and anti-reflection (AR) dielectric multilayer optical coatings on the facets. The device is a continuous wave, buried heterostructure QCL emitting at 4.5 μm. Its cavity length is 6 mm and the nominal reflectivity values are $R_1 = 0.95$ (HR) and $R_2 = 0.01$ (AR). The patterns measured by LIIRR at f_B and $2f_B$ when the laser operates in the frequency comb regime are shown in Fig. 4a. They exhibit asymmetric profiles that are clearly different from those of uncoated Fabry-Perot cavities (cf. Fig. 2b): the beat note power, which is proportional to the oscillating component of the intracavity intensity, is strong in proximity of the AR facet and weak on the HR side. This general behavior, which is due to the traveling wave character of the cavity, is the one expected for HR/AR devices [21] and is also predicted by the analytical model based on Eq. 1. The agreement between the model and the experiments is very good for the pattern at f_B, while for the one at $2f_B$ there is an experimental dip close to the AR facet which is not predicted theoretically. The reason for this dip is not clear and remains to be further investigated. It may be an artifact due to a residual trace of the optical coating lying on the top of the laser ridge, which can add a capacitance between the probe and the top electrode affecting the microwave measurement.

Next, we investigate the effect that a gap etched in a QCL ridge has on light propagating inside the cavity. The cavity is symmetric, with HR coatings on both facets, and is 8 mm long. The width of the gap is 400 μm (much larger than the laser wavelength, which is 9 μm) and its depth does not extend to the active region of the laser (Fig. 4b), i.e., it does not create two coupled sub-cavities but it defines two contact sections with an open-circuit resistance of 250 Ω. Similar geometries are often used

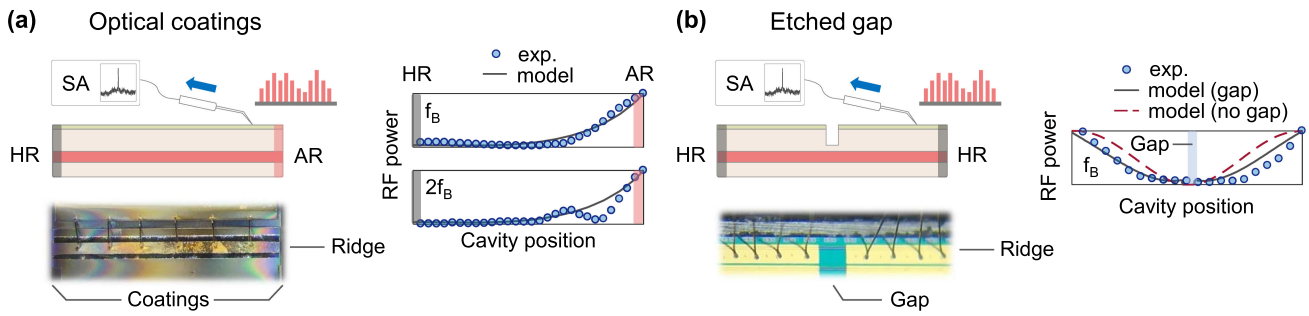

Fig. 4. Oscillatory gratings in structured cavities of quantum cascade lasers. (a) Measured microwave gratings at the fundamental (f_B) and second-harmonic ($2f_B$) beat note of a quantum cascade laser operating in the frequency comb regime. The device has an asymmetric Fabry-Perot cavity defined by a high-reflectivity (HR) and an anti-reflection (AR) dielectric multilayer coating. Also shown is a top view microscope image of the device showing some residual traces of the optical coatings on the electrodes. (b) Measured microwave grating at f_B in a quantum cascade laser with an etched gap and a symmetric HR/HR cavity. Also shown is a top view microscope image of part of the device. The width of the gap is 400 μm and the length of the cavity is 8 mm. Both in (a) and (b) are also shown the predictions of models described in the text.

in devices for active [22] or injection locking [23] experiments in order to separate a radio frequency section from a DC bias section. The experimental profile measured by LIIRR at f_B is shown in Fig. 4b. A clear flattening of the profile is observed as compared to that of symmetric cavities without gap (cf. dashed line in Fig. 4b). This is a remarkable effect because it shows that the gap affects the intracavity power distribution on a spatial scale of several millimeters, which is much longer than the width of the gap. It can be explained considering that the gap acts as a loss section due to the voltage drop occurring in this region of the cavity. Light waves passing through the gap experience a strong suppression because of optical absorption and their amplitude re-increases only after propagating over a long distance across the cavity. To confirm this hypothesis we carry out numerical simulations based on a space- and time-domain model of transport and recombination in the QCL active region [24]. The voltage drop in the gap region is modeled assuming a voltage profile along the cavity given by

$$V(x) = (V_{\mathrm{DC}} - V_{\mathrm{gap}})|\tanh(5x/w_{\mathrm{gap}})| + V_{\mathrm{gap}} \qquad (5)$$

where V_{DC} and V_{gap} are parameters defining the biases on the contact sections and at the center of the gap, respectively, w_{gap} is the width of the gap, and $x = 0$ corresponds to the center of the cavity. In the following we provide for completeness all the simulation parameters, even though the essential feature that is studied here is predicted regardless of the specific QCL parameters, as long as a sizeable voltage drop occurs in the gap. Following the notation of Ref. [24], the parameters are: 1) bias profile: $V_{\mathrm{DC}} = 0.9$, $V_{\mathrm{gap}} = 10^3$, $w_g = 400$ μm (voltages are normalized to the threshold bias, $V_{\mathrm{th}} = -7.74$ kV/cm, and the reference $V = 0$ is defined as the alignment condition of the injector state with the upper laser state); 2) resonant tunneling parameters entering the injection current (Eq. (2) in Ref. [24]): the coupling energy $\Omega = 1.36$ meV, level broadening $\gamma = 5.44$ meV, the tunneling barrier width between upper laser state and injector states $\delta = 10.1$ nm; 3) relaxation timescales: an upper to lower laser state relaxation time $T_{ul} = 1$ ps, upper laser to injector state relaxation time $T_{ug} = 1.5$ ps, lower laser to injector state relaxation time $T_{lg} = 0.25$ ps, dephasing time $T_2 = 0.26$ ps, diffusion coefficient $D = 77$ cm^2/s; 4) optical parameters: the effective refractive index n =3.3, modal waveguide loss for the field $l_w = 0.9$ cm^{-1}, modal overlap factor $\Gamma = 0.41$, the dipole matrix element of the gain transition $d = e \times 2.04$ nm, central laser wavelength $\lambda_0 = 9.0$ μm; 5) QCL structure parameters: the length of one period $L_p = 580$ Å, doping density $n_{\mathrm{doping}} = 1.1 \times 10^{11}$ cm^{-2}, electron temperature $T_e = 289$ K, cavity length $L = 8$ mm. The pattern of beat note power obtained from the simulations of the gap device exhibits a profile in good agreement with the experiments (Fig. 4b), thus confirming that the voltage drop occurring in the gap is sufficient to explain the observed flattening of the intracavity power distribution across the cavity. Overall these results demonstrate that LIIRR can become a new tool to characterize intensity field variation in laser frequency combs.

C. Microwave Propagation

As already explained in Section II-A, microwaves originate from a radio frequency voltage across the active region of the laser frequency comb, which is induced by photon-driven transport. A good question to ask is whether such modulation also causes in-plane current oscillations. Put differently, does the laser act as a transmission line allowing microwaves to propagate along the cavity? This is an important aspect to investigate for two reasons. First, microwave propagation would affect the profiles of the microwave gratings, complicating the use of LIIRR as a characterization method of the intracavity intensity. Second, it could contribute to phase-locking of the optical modes [25], thus it would have to be taken into account in the modeling of frequency combs.

To discuss microwave propagation effects in QCLs, let us start by considering the basic case of microwave coplanar waveguides (CPWGs). These are electrical planar transmission lines designed to convey microwave signals with minimal losses. They can also act as microwave resonators, which find use in solid-state quantum computing [26]. A first method to characterize a microwave CPWG is to use a vector network analyzer (VNA) giving access to the experimental scattering parameters, from which the quality factor of the resonator can be deduced [26]. As an example, we present in Fig. 5a the characterization of a

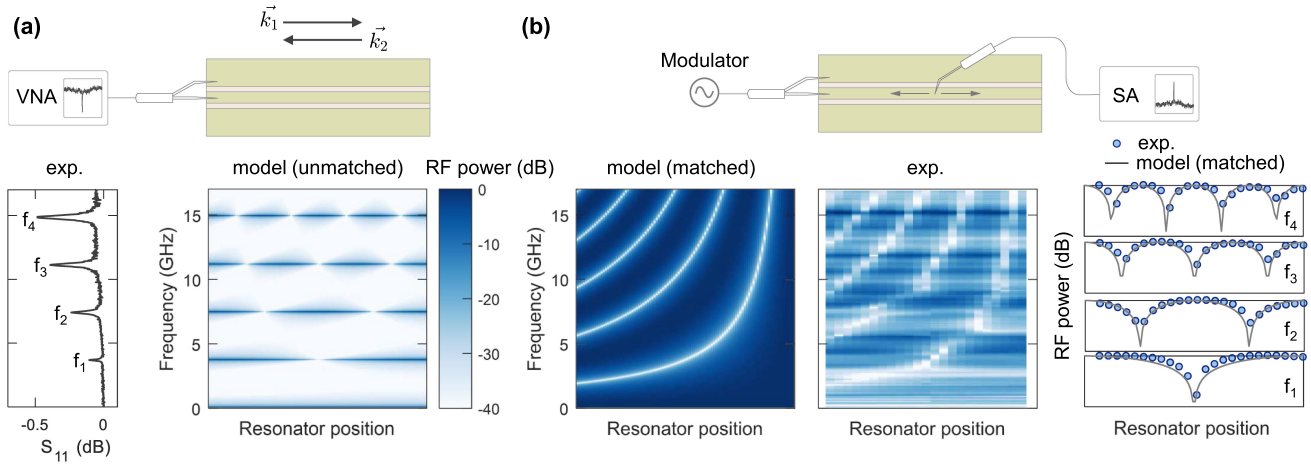

Fig. 5. Characterization of a microwave coplanar waveguide. (a) A vector network analyzer (VNA) is connected to the coplanar waveguide via a signal-ground probe. The signal-pin is lifted few μm above the central conductor of the waveguide adding a coupling capacitance that makes the waveguide act as a resonator. The measurement of the reflection coefficient (S_{11}) shows the first four resonant frequencies of the waveguide. Also shown is the prediction of a model based on the telegrapher's equations for the spatial profiles of the microwave resonant modes. (b) A second characterization method of the coplanar waveguide. A generator sends a microwave tone to the waveguide via a signal-ground probe. The probe is impedance matched to the waveguide and both of its pins are in contact with the conductors of the waveguide making this a continuation of the transmission line constituted by the signal-probe and its radio frequency cable. A signal-only probe is scanned across the resonator to measure the local microwave power using a spectrum analyzer (SA). Standing-waves are mapped at several frequencies of the modulator in the range 0–17 GHz, and agree with the predictions of the model based on the telegrapher's equations. The colorbar is the same as in (a). Also shown are the 1D cuts of the experimental and model maps at the resonant frequencies of the coplanar waveguide (f_1 to f_4). The same characterization methods were carried out on QCLs but did not reveal any resonant or standing-wave feature at microwave frequencies.

25 mm-long microwave CPWG. A signal-ground (SG) probe is used to connect the VNA to the CPWG. The S-pin is lifted from the central conductor by few μm, effectively adding a capacitance that allows one to use the CPWG as a resonator. After calibration of the system on an alumina calibration substrate, the measurement of the reflection coefficient (S_{11}) reveals the resonances of the CPWG. They appear as dips lying at multiples of the free spectral range of the resonator $f_n = c/(2nL)$, where the microwave refractive index is $n = 1.61$. Also shown in Fig. 5a are the first four resonant modes of the CPWG calculated using from the telegrapher's equations [27], assuming the right end of the CPWG as an open circuit and a strong impedance mismatch between the generator and the waveguide ($Z_g/Z_w = 10^3$, where Z_g and Z_w are the impedances of the generator and the waveguide, respectively).

A second method that can be used to characterize the CPWG is a scanning probe technique (Fig. 5b). The SG probe sends the signal generated from a radio frequency modulator to the CPWG. In this case both the S- and G-pin of the probe are in contact with the central conductor of the CPWG. A second signal-only probe is used to map the local microwave power along the transmission line. This is repeated for many different frequencies of the modulator. The experimental result shows minima whose position shifts across the resonator cavity as a function of frequency (Fig. 5b). This effect is reproduced by the model based on the telegrapher's equations, assuming impedance matching between the generator and the waveguide ($Z_g = Z_w$). This implies that the coplanar waveguide acts as a continuation of the much longer transmission line constituted by the SG probe and its radio frequency cable, explaining why standing waves are observed at essentially all frequencies, rather than just at the resonant frequencies of the CPWG (cf. Fig. 5a).

We carried out measurements on mid-infrared QCLs based on both types of characterization methods just described. Several devices were tested with buried heterostructure and ridge geometry. In no case resonances or microwave standing-waves were observed. This can be understood considering that the doped dielectric of QCL heterostructures and the narrow width of their ridges cause strong losses at microwave frequencies, despite their geometry being similar to that of microwave microstrip transmission lines [30]. Calvar *et al.* calculated by means of finite element simulations an attenuation coefficient of 90 cm^{-1} at 13 GHz for standard mid-infrared buried heterostructure QCLs, corresponding to a propagation length of only 110 μm [31]. This is several orders of magnitude shorter than the typical propagation length of microwave CPWGs (e.g., 8 m in the sample reported in Fig. 5) and implies that standard, mm-long QCLs cannot act as microwave resonators. Therefore we conclude that microwave gratings observed in laser frequency combs are not affected by microwave propagation effects in the laser microstrip.

This conclusion, however, does not exclude that microwaves generated by the laser frequency comb may propagate in other areas of the laser chip different from the microstrip. We next show how the intrinsic microwave gratings may be affected by structuring the layout of the surrounding electrical contacts. The device geometry used for this demonstration is shown in Fig. 6. The laser is a mid-infrared, buried heterostructure, uncoated QCL with a cavity length $L = 6$ mm (labeled 'TL-4.6' in Ref. [32]). Its top pad, which is connected to the top electrode of the laser, is designed to be asymmetric with respect to the center of the cavity and lies on top of an undoped dielectric SiC substrate. The length of the pad is $L_{\mathrm{pad}} = 2.7$ mm. The microwave gratings mapped along the cavity when the laser operates in the

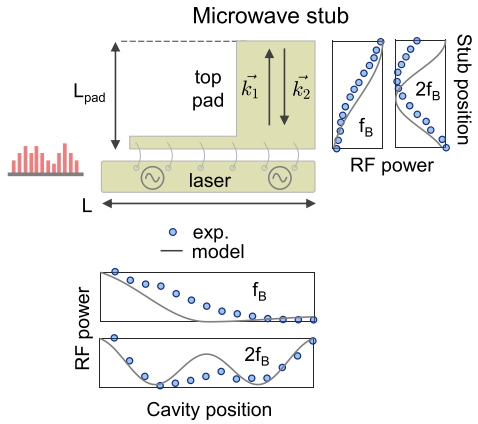

Fig. 6. Schematic of a laser with an asymmetric pad connected to its top electrode. This pad acts as a microwave stub suppressing the microwave power at certain frequencies and at certain positions in the laser cavity. Microwave gratings measured at f_B and $2f_B$ when the laser operates in the frequency comb regime are shown, together with the profiles of microwave power mapped on the pad at the same frequencies and in the same conditions. Also shown are the profiles calculated from a model described in the text.

frequency comb regime exhibit a feature which is not observed in devices with ordinary contact pads (Fig. 6). The profile at f_B is strongly asymmetric – differently from what is expected for an uncoated cavity (cf. Fig. 2b) – presenting a minimum at the facet close to the top pad and a maximum at the opposite facet. On the other hand, the microwave grating measured at $2f_B$ is not asymmetric and shows the usual profile (cf. Fig. 2b). This effect is observed in several devices with this contact geometry, and cannot arise from the laser cavity itself since this is symmetric. Moreover, it is an anomaly that is frequency dependent, as it does not affect all beat gratings. There are no sources of asymmetry in the device other than the top pad, thus one can only suspect a microwave – rather than an optical – effect.

This behavior can be understood as being caused by a resonant microwave stub effect, i.e., we consider the top pad as a transmission line that is connected only on one end to the laser – acting as a microwave generator due to the beating of its optical modes – and with the free end left open-circuit. The refractive index of the SiC substrate under the pad is $n_{\text{pad}} \approx 3.1$ [33], close to that of the QCL waveguide $n = 3.23$ [32]. Noting that the length of the pad is designed to be $L_{\text{pad}} \approx L/2 = \lambda_B/4 = \lambda_{2B}/2$, where λ_B and λ_{2B} are the wavelengths of the fundamental and second order beat waves, the pad should act similarly to a quarter- and half-wavelength stub at these frequencies. Solving the telegrapher's equations for the stub we obtain the theoretical profiles shown in Fig. 6 giving the microwave power as a function of the position on the stub. These profiles are also experimentally measured by scanning a microwave probe on top of the pad and are found to exhibit similar features to the model predictions. We observe standing-waves both at f_B and $2f_B$, with a node (antinode) at f_B ($2f_B$) on the end of the stub connected to the laser. These results indicate that the asymmetry of the grating at f_B mapped on the laser is caused by a partial suppression of microwave power due to the pad acting as a quarter-wavelength stub. (For the corresponding theoretical profile in Fig. 6 it was assumed a power suppression factor of 10^{-1}.) At the same time, the pad does not affect the grating at $2f_B$, since it acts as a half-wavelength stub.

Given that microwave gratings can be influenced by the geometry of the laser pad, one may wonder whether this may also play a role on frequency comb operation. Indeed, suppression of the fundamental beat note in part of the laser cavity should be an obstacle for the formation of an optical frequency comb spaced by f_B. We advance the hypothesis that the asymmetric pad geometry shown in Fig. 6 favors longitudinal mode skipping. An empirical support for this argument is that in all devices with this geometry (5 were studied so far) harmonic frequency combs with an intermodal spacing of several free spectral ranges were observed over a certain current range [32], [34]–[36]. (Note, however, that harmonic frequency combs were also observed in lasers with symmetric pads. Thus asymmetric pads may be a sufficiency but not necessary condition for harmonic comb operation.) Future investigations will allow to verify this hypothesis. If proven correct, laser contact pad layout may become a new knob controlling frequency comb operation.

IV. Applications in Science and Technology

The microwave gratings effects investigated in this work open up novel applications in laser science and technology, which have just started being explored. In this last section we will present the first uses of these phenomena, which will serve also to give an outlook on possible future directions of this research. In terms of science applications, LIIRR could become a new characterization tool for semiconductor lasers and we will show that this technique can also be applied to ICLs. Recent works exploiting the knowledge of microwave gratings in QCL frequency combs will be presented. In terms of technology applications, the interaction of light and microwaves studied here defines a new laser operating mode which allows for novel hybrid electronic-photonic devices, which will be introduced.

A. Gratings in Interband Cascade Lasers

Even though all the spatiotemporal phenomena illustrated in Section III were shown to occur in QCLs, they do not have to be intended as exclusive of this type of laser. Here we show that similar effects can also occur in ICLs.

ICLs are semiconductor lasers relying on interband transitions to provide optical gain and can operate in a large part of the mid-infrared region of the electromagnetic spectrum [37], [38]. Despite the long lifetime of interband transitions, ICLs can behave as fast gain media, i.e., the gain medium can respond to intermodal beatings. This was illustrated recently by modulation experiments and the demonstration of self-starting frequency combs in ICLs, which present features similar to QCL frequency combs [39].

Since the electronic response of ICLs is sufficiently fast to respond to the beating of the optical modes, microwave generation inside the laser should occur, enabling grating effects similar to those observed in QCLs. We studied an ICL with a cavity length of 3 mm. For the passivation a 1.6 μm thick SiN insulating layer was deposited over the entire chip to improve its radio frequency

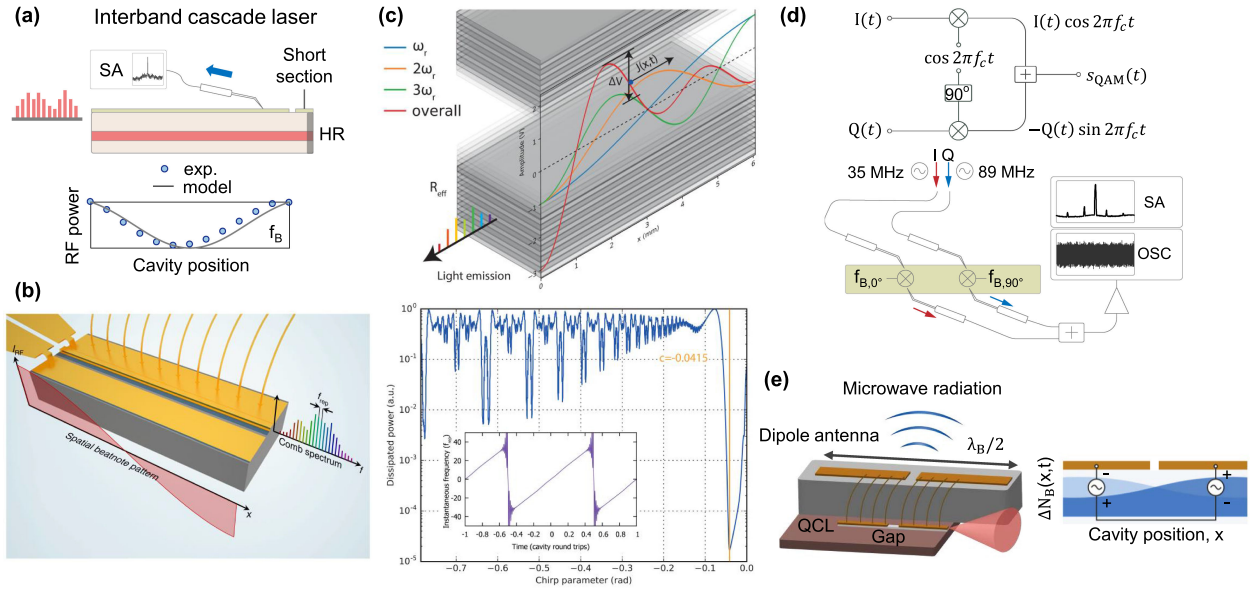

Fig. 7. Uses of microwave gratings in science and technology. (a) Microwave grating mapped at the fundamental beat note frequency of an interband cascade laser. (b) Coherent injection locking of a semiconductor laser frequency comb. The external modulator injects a radio frequency signal at the edge of the cavity, corresponding to an antinode of the inherent microwave grating of the laser. (c) Microwave gratings in a QCL frequency comb induce in plane currents ($J(x,t)$), which dissipate laser power by ohmic losses. The gratings at the fundamental (ω_r), second ($2\omega_r$) and third harmonic ($3\omega_r$) beat note frequencies are shown (top). The dissipated power depends on the chirp coefficient (bottom), which parametrizes the phase relationship of the comb modes. (d) Laser operating as a microwave quadrature mixer for quadrature amplitude modulation. The block diagram (top) shows the working principle of a generic quadrature mixer. Two baseband signals, $I(t)$ and $Q(t)$, are mixed in-phase and in-quadrature with a carrier at frequency f_c. The resulting signals are superimposed giving the QAM waveform, s_{QAM}. The realization of a QAM mixer using a QCL is also shown (bottom): two microwave probes inject two tones of different frequencies, I and Q, in a QCL at positions where the laser beat note is dephased by 90°. The mixed signals are then extracted with two additional probes, combined with a 3-dB coupler and recorded using a spectrum analyzer (SA) and a mixed-signal oscilloscope (OSC). (e) Laser frequency comb operating as a radio transmitter. The device design employs a gap to electrically separate the radio frequency signals generated in the two halves of the cavity at the fundamental beat note of the laser. This enables emission of microwaves into free space using a dipole antenna integrated on the chip of length $\lambda_B/2$, where λ_B is the wavelength corresponding to the fundamental beat note. (b) Reprinted by permission from Macmillan Publishers Ltd.: J. Hillbrand, A. M. Andrews, H. Detz, G. Strasser, and B. Schwarz, Nature Photonics 13, 101 (2019) [23]. Copyright 2019. (c), (d) Reprinted with permission from Ref. [11], [28]. Copyright 2018 Optical Society of America. (e) Reprinted with permission from Ref. [29].

properties. The device, which was initially designed for dispersion compensation experiments, consists of a long and a short section. The cavity is uncoated on the long section side and HR-coated on the short section side using a SiN/Ti/Au coating. The DC bias set on the short section is slightly different with respect to that applied to the long section: this allows to match the effective reflectivity of the coated end of the cavity to that of the uncoated facet (Fig. 7a), making the laser cavity effectively symmetric for the optical field. This is possible because the gain coefficient of the short ICL section can be continuously tuned from negative (absorption) to positive (gain) values via the bias.

The laser operates in free-running mode. Despite the beat note being rather broad (MHz linewidth) a microwave grating could be measured by the scanning probe technique at the fundamental beat note frequency of the laser ($f_B = 11.6$ GHz). The experimental result is shown in Fig. 7a and agrees well with the pattern expected for a symmetric Fabry-Perot cavity. Higher order beat notes could not be measured due to the low signal-to-noise ratio at frequencies above 20 GHz, but may be studied in the future in devices with longer cavities and smaller free spectral range.

B. Gratings and Optical Frequency Combs

The knowledge of microwave gratings was recently used in the demonstration of coherent injection locking of QCL and ICL frequency combs [23], [39]. This technique enables the all-electrical generation of robust frequency combs that are not destabilized by optical feedback [23]. It uses an external radio frequency modulator to inject a signal close to the roundtrip frequency of the laser and lock its optical modes [40]. In general, it is not granted that the entire spectrum ends up being locked. The recent achievement used a linear phase-sensitive autocorrelation technique [41] to measure the intermodal phase relationship of the laser and prove that all modes can be coherently locked together, thus forming an electrically-stabilized frequency comb. A key expedient to achieve this result consisted in placing the modulator probe at the edge of the cavity (Fig. 7b). As illustrated in Section III-A, this arrangement maximizes the efficiency of injection locking, which varies along the cavity as the profile of the microwave grating oscillating at the roundtrip frequency of the laser (Fig. 3c). Moreover, since microwaves do not propagate across the laser cavity (Section III-C) – due to the strong radio frequency attenuation of the doped dielectric medium – the action of the modulator can essentially be considered as localized.

Microwave gratings effects were also brought into play in the interpretation of recent measurements revealing the temporal character of self-starting QCL frequency combs [28]. In these studies it was shown that the spectra of such lasers exhibit parabolic phase profiles corresponding to linear frequency chirps in the time domain, i.e., the instantaneous frequency of

the laser sweeps across the whole spectral range during one period of the comb. The spectral phases were parametrized by a chirp coefficient c giving a phase profile $\exp(icn^2)$ – where n is the mode index relative to the primary mode – and it was observed that the experimental chirp coefficient minimizes intensity modulation at the laser output, as required for a laser with ultrafast gain dynamics. However, it was also found by calculation that other chirp parameters potentially exist, which can minimize intensity modulation as well as the experimental c coefficient. These other parameters correspond to higher order linear chirps, i.e., multiple linear frequency sweeps over one period of the comb. To explain why the laser favors the lowest order linear chirp observed in the experiment, rather than high order linear chirps, the authors proposed to consider the role of microwave gratings in the frequency comb operation. It was pointed out that the radio frequency voltage profile associated with these gratings induces in-plane currents (Fig. 7c, top), which in turn dissipate laser power due to losses in the doped cladding and contact layers. Based on a model that considered all the possible beatings among the laser modes, the authors calculated the power dissipated by ohmic losses as a function of the chirp coefficient (Fig. 7c, bottom), obtaining that high order chirp parameters give a much higher dissipation – by a factor of 100 or more – than the lowest order linear chirp. This result suggested that the experimental c coefficient is therefore favored by the laser as it minimizes not only intensity modulation but also ohmic losses.

C. Hybrid Electronic-Photonic Devices

The light-matter interaction investigated in this work defines a novel laser operating mode which allows for a new class of hybrid electronic-photonic devices. Exploiting the phase of the oscillatory gratings (Fig. 2b), it has been shown that a semiconductor laser can act as a microwave quadrature mixer for quadrature amplitude modulation (QAM) [11]. This is a widely used scheme in modern communications. A block diagram illustrating its working principle is shown in Fig. 7d (top). Two baseband signals, $I(t)$ and $Q(t)$, are mixed in phase and in quadrature (i.e., 90° phase shift) with a carrier at frequency f_c. After subsequent summation, the QAM signal $s_{\mathrm{QAM}}(t)$ is obtained. Since in this method both the amplitude and phase of the carrier are modulated, QAM allows to double the spectral efficiency of the transmitted signal. A quadrature mixer was realized using a QCL frequency comb by injecting two different tones, I and Q, at positions in the laser cavity where the fundamental beat note is dephased by 90° (Fig. 7d, bottom). The signals mixed with the laser beat note were then extracted from the laser, superimposed and recorded with a specrum analyzer and a mixed-signal oscilloscope. After coherent signal demodulation, it was shown that the two initial input signal could be successively retrieved, proving that the I and Q signals are indeed summed in quadrature thanks to the phase profile of the inherent microwave grating of the laser.

This approach also enabled another type of device, which was named laser radio transmitter [29]. This idea arose by looking at laser oscillatory gratings as an ensemble of radio frequency generators placed along the cavity and connected in parallel (Fig. 7e). Usually the top electrode of a semiconductor laser consists of an electrically continuous metal contact effectively connecting these radio frequency generators and thus preventing the device from radiating. It was demonstrated that waveguide and radio frequency engineering of the laser allow to exploit the oscillatory gratings to feed a dipole antenna integrated on the chip, enabling emission of radio waves into free space. The beat note frequency itself can be tuned by modulating the laser current, thus the laser acquires a new functionality: it becomes a radio transmitter capable of wireless communication at a carrier frequency given by the comb repetition rate. This proof-of-concept demonstration was done at microwave frequencies but holds the potential to be extended to terahertz frequencies by operating the laser in a harmonic frequency comb regime [34] with a wide intermodal spacing. The potential advantages of the envisioned room-temperature QCL terahertz transceiver as compared to purely electronic or other hybrid electronic-photonic counterparts are the emission of narrow tones over a large frequency range [35] and the hybrid functionality of carrier generator and quadrature mixer within a single body, which will considerably limit the transceiver unit footprint.

ACKNOWLEDGMENT

M. Piccardo and A. Amirzhan would like to thank J. Waissman and A. Talanov (Philip Kim group, Harvard University) for lending a VNA. Any opinions, findings, conclusions, or recommendations expressed in this material are those of the authors and do not necessarily reflect the views of the National Science Foundation.

REFERENCES

[1] H. J. Eichler, P. Gunter, and D. W. Pohl, *Laser-Induced Dynamic Gratings*. New York, NY, USA: Springer, 1986.
[2] J. P. Huignard, J. P. Herriau, and T. Valentin, "Time average holographic interferometry with photoconductive electrooptic $Bi_{12}SiO_{20}$ crystals," *Appl. Opt.*, vol. 16, no. 11, pp. 2796–2798, 1977.
[3] J. P. Huignard, J. P. Herriau, and F. Micheron, "Coherent selective erasure of superimposed volume holograms in $LiNbO_3$," *Appl. Phys. Lett.*, vol. 26, no. 5, pp. 256–258, 1975.
[4] G. T. Sincerbox and G. Roosen, "Opto-optical light deflection," *Appl. Opt.*, vol. 22, no. 5, pp. 690–697, Mar. 1983.
[5] A. Korpel, R. Adler, and B. Alpiner, "Direct observation of optically induced generation and amplication of sound," *Appl. Phys. Lett.*, vol. 5, no. 4, pp. 86–88, 1964.
[6] L. Xiong *et al.*, "Photoacoustic trace detection of gases at the parts-per-quadrillion level with a moving optical grating," *Proc. Nat. Acad. Sci. USA*, vol. 114, no. 28, pp. 7246–7249, 2017.
[7] L. Yang *et al.*, "Doppler velocimetry of spin propagation in a two-dimensional electron gas," *Nature Phys.*, vol. 8, pp. 153–157, Dec. 2011.
[8] S. Odoulov *et al.*, "Interference and holography with femtosecond laser pulses of different colours," *Nature Commun.*, vol. 6, Feb. 2015, Art. no. 5866.
[9] P. Peterka *et al.*, "Dynamic gratings induced by mode instabilities in fiber lasers," in *Proc. 21st Czech-Polish-Slovak Opt. Conf. Wave Quantum Aspects Contemporary Opt.*, 2018, vol. 10976, Paper 109760H.
[10] P. Bardella, L. L. Columbo, and M. Gioannini, "Self-generation of optical frequency comb in single section quantum dot Fabry–Perot lasers: A theoretical study," *Opt. Express*, vol. 25, no. 21, pp. 26 234–26 252, Oct. 2017.
[11] M. Piccardo *et al.*, "Time-dependent population inversion gratings in laser frequency combs," *Optica*, vol. 5, no. 4, pp. 475–478, Apr. 2018.
[12] S. Adam, *Microwave Theory and Applications*. Los Altos, CA, USA: Adam Microwave Consulting, 1992.

[13] J. Faist *et al.*, "Quantum cascade laser frequency combs," *Nanophotonics*, vol. 5, no. 2, pp. 272–291, 2016.
[14] A. E. Siegman, *Lasers*. Sausalito, CA, USA: Univ. Sci. Books, 1986.
[15] M. Armand, "On the output spectrum of unlocked driven oscillators," *Proc. IEEE*, vol. 57, no. 5, pp. 798–799, May 1969.
[16] P. Gellie *et al.*, "Injection-locking of terahertz quantum cascade lasers up to 35 GHz using RF amplitude modulation," *Opt. Express*, vol. 18, no. 20, pp. 20799–20816, Sep. 2010.
[17] H. L. Stover, "Theoretical explanation for the output spectra of unlocked driven oscillators," *Proc. IEEE*, vol. 54, no. 2, pp. 310–311, Feb. 1966.
[18] T. S. Mansuripur, "The effect of intracavity field variation on the emission properties of quantum cascade lasers," Ph.D. dissertation, Dept. Phys., Harvard University, Cambridge, MA, USA, 2016.
[19] L. W. Hillman, J. Krasinski, J. A. Yeazell, and C. R. Stroud, "Intracavity power measurement by Rayleigh scattering," *Appl. Opt.*, vol. 22, no. 22, pp. 3474–3474, Nov. 1983.
[20] L. J. P. Ketelsen, I. Hoshino, and D. A. Ackerman, "The role of axially nonuniform carrier density in altering the TE-TE gain margin in InGaAsP-InP DFB lasers," *IEEE J. Quantum Electron.*, vol. 27, no. 4, pp. 957–964, Apr. 1991.
[21] W. C. W. Fang, C. G. Bethea, Y. K. Chen, and S. L. Chuang, "Longitudinal spatial inhomogeneities in high-power semiconductor lasers," *IEEE J. Sel. Topics Quantum Electron.*, vol. 1, no. 2, pp. 117–128, Jun. 1995.
[22] C. Y. Wang *et al.*, "Mode-locked pulses from mid-infrared quantum cascade lasers," *Opt. Express*, vol. 17, no. 15, pp. 12929–12943, Jul. 2009.
[23] J. Hillbrand, A. M. Andrews, H. Detz, G. Strasser, and B. Schwarz, "Coherent injection locking of quantum cascade laser frequency combs," *Nature Photon.*, vol. 13, pp. 101–104, Dec. 2019.
[24] Y. Wang and A. Belyanin, "Active mode-locking of mid-infrared quantum cascade lasers with short gain recovery time," *Opt. Express*, vol. 23, no. 4, pp. 4173–4185, Feb. 2015.
[25] F. Wang *et al.*, "Generating ultrafast pulses of light from quantum cascade lasers," *Optica*, vol. 2, no. 11, pp. 944–949, Nov. 2015.
[26] S. Putz, *Circuit Cavity QED With Macroscopic Solid-State Spin Ensembles*. New York, NY, USA: Springer, 2017.
[27] J. D. Kraus, *Electromagnetics*, 3rd ed. New York, NY, USA: McGraw-Hill, 1984.
[28] M. Singleton, P. Jouy, M. Beck, and J. Faist, "Evidence of linear chirp in mid-infrared quantum cascade lasers," *Optica*, vol. 5, no. 8, pp. 948–953, Aug. 2018.
[29] M. Piccardo *et al.*, "Radio frequency transmitter based on a laser frequency comb," in *Proc. Natl. Acad. Sci. U.S.A 201903534*, Apr. 2019.
[30] W. Maineult *et al.*, "Microwave modulation of terahertz quantum cascade lasers: A transmission-line approach," *Appl. Phys. Lett.*, vol. 96, no. 2, 2010, Art. no. 021108.
[31] A. Calvar *et al.*, "High frequency modulation of mid-infrared quantum cascade lasers embedded into microstrip line," *Appl. Phys. Lett.*, vol. 102, no. 18, 2013, Art. no. 181114.
[32] T. S. Mansuripur *et al.*, "Single-mode instability in standing-wave lasers: The quantum cascade laser as a self-pumped parametric oscillator," *Phys. Rev. A*, vol. 94, no. 6, Dec. 2016, Art. no. 63807.
[33] L. Patrick and W. J. Choyke, "Static dielectric constant of SiC," *Phys. Rev. B*, vol. 2, no. 6, pp. 2255–2256, Sep. 1970.
[34] D. Kazakov *et al.*, "Self-starting harmonic frequency comb generation in a quantum cascade laser," *Nature Photon.*, vol. 11, pp. 789–792, 2017.
[35] M. Piccardo *et al.*, "Widely tunable harmonic frequency comb in a quantum cascade laser," *Appl. Phys. Lett.*, vol. 113, no. 3, Jul. 2018, Art. no. 031104.
[36] M. Piccardo *et al.*, "The harmonic state of quantum cascade lasers: Origin, control, and prospective applications [Invited]," *Opt. Express*, vol. 26, no. 8, pp. 9464–9483, Apr. 2018.
[37] R. Q. Yang and S. S. Pei, "Novel type-II quantum cascade lasers," *J. Appl. Phys.*, vol. 79, no. 11, pp. 8197–8203, Jun. 1996.
[38] I. Vurgaftman *et al.*, "Interband cascade lasers," *J. Phys. D, Appl. Phys.*, vol. 48, no. 12, 2015, Art. no. 123001.
[39] B. Schwarz *et al.*, "A monolithic frequency comb platform based on interband cascade lasers and detectors," 2018, arXiv:1812.03879.
[40] M. R. St-Jean *et al.*, "Injection locking of mid-infrared quantum cascade laser at 14 GHz, by direct microwave modulation," *Laser Photon. Rev.*, vol. 8, no. 3, pp. 443–449, May 2014.
[41] D. Burghoff *et al.*, "Evaluating the coherence and time-domain profile of quantum cascade laser frequency combs," *Opt. Express*, vol. 23, no. 2, pp. 1190–1202, Jan. 2015.

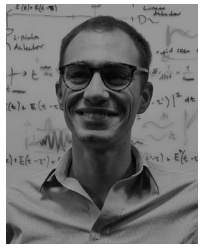

Marco Piccardo received the B.Sc. degree in physics from the Universitá degli Studi di Torino, Turin, Italy, the M.Sc. degree in physics from the École Normale Supérieure and École Polytechnique, Paris, France, and the Ph.D. degree in physics from the École Polytechnique advised by C. Weisbuch, J. Peretti, and L. Martinelli. His main focus was on the investigation of the fundamental electronic processes responsible for the drop in efficiency of nitride light-emitting diodes at high-current operation. He is currently a Postdoctoral Research Fellow with the group of F. Capasso at Harvard University, Cambridge, MA, USA, exploring novel electronic and photonic properties of laser frequency combs.

Dmitry Kazakov was born in Moscow, Russia. He received the B.Sc. degree in electrical engineering from the Swiss Federal Institute of Technology, Zurich, Switzerland. He dropped out of the master's program in electrical engineering to start the Ph.D. degree in applied physics with the group of Prof. F. Capasso at Harvard University, Cambridge, MA, USA. During his undergraduate degrees, he joined the Lab of Prof. J. Faist to work on quantum cascade laser frequency combs for spectroscopy applications. He is currently investigating dynamic gratings in laser frequency combs.

Benedikt Schwarz received the M.Sc. (with honors) degree in microelectronics from TU Wien, Vienna, Austria, in 2011, investigating quantum effects, discrete dopants, and oxide traps in nanoscaled metal–oxide–semiconductor transistors, and the Ph.D. degree, in 2015, developing a monolithically integrated lab-on-a-chip using quantum cascade technology. He is currently a Visiting Researcher with Prof. F. Capasso at Harvard University, Cambridge, MA, USA, and a Principal Investigator with TU Wien, where he is working on RF detectors, fundamentals of quantum cascade laser (QCL) and interband cascade laser (ICL) frequency combs, and monolithic integration of mid-infrared spectrometers.

Paul Chevalier received the engineering degree and the Ph.D. degree in physics from École Polytechnique, Palaiseau, France, in 2012 and 2015, respectively. He is currently a Postdoctoral Researcher with the Prof. F. Capasso Group at Harvard School of Engineering and Applied Science, Cambridge, MA, USA. His research interests include gas and liquid-phase spectroscopy, quantum cascade lasers, THz generation, and polarization imaging.

Arman Amirzhan was born in Almaty, Kazakhstan, in 1995. He received the B.Eng. degree in materials science and engineering from the Imperial College London, London, U.K., in 2016. He is currently working toward the Ph.D. degree in applied physics at the School of Engineering and Applied Science, Harvard University, Cambridge, MA, USA. From 2016 to 2017, he was a Research Assistant with the Materials Department, Imperial College London, where he worked on room temperature masers developing low-cost electron paramagnetic resonance (EPR) spectrometer together with Prof. M. Oxborrow. His current research focuses on developing THz devices.

Johannes Hillbrand received the master's degree in physics from the Swiss Federal Institute of Technology (ETH), Zurich, Switzerland, in 2017. He is currently working toward the Ph.D. degree in electrical engineering with the group of Prof. G. Strasser at TU Vienna, Vienna, Austria. During his master's thesis, he joined the group of Prof. J. Faist to work on quantum cascade laser frequency combs. His work focuses on high-speed mid-infrared photonics, in particular quantum cascade and interband cascade structures for monolithic integration of lasers and detectors.

Sultan Z. Almutairi received the bachelor's degree in physics and mathematics from the King Fahd University of Petroleum and Minerals, Dhahran, Saudi Arabia, in 2014, and the master's degree in physics from Texas A&M University, College Station, TX, USA, in 2017, where he is currently working toward the Ph.D. degree with the Department of Physics.

Yongrui Wang received the Ph.D. degree in physics from the Texas A&M University, College Station, TX, USA, in 2015. Since 2010, he has been first a Research Assistant and then a Postdoctoral Research Associate with the Department of Physics and Astronomy, Texas A&M University, working on theoretical calculations about optical properties of semiconductor structures and devices. His research interests include mode locking in quantum cascade lasers, nonlinear optics, and many-body interaction in semiconductor structures.

Feng Xie (M'09) received B.S. and M.S. degrees in physics from the University of Science and Technology of China, Hefei, China, in 2000 and 2003, respectively, and the Ph.D. degree in applied physics from Texas A&M University, College Station, TX, USA, in 2008. He joined Corning Incorporated in 2008 as a Research Scientist with the Department of Semiconductor Technologies, and was promoted to a Senior Research Scientist in 2011. The department was acquired by Thorlabs Quantum Electronics (TQE), Inc., in 2015, and then, he joined TQE. His research interests include mid/far-infrared semiconductor laser and optoelectronics devices, including high-performance and nonlinear quantum cascade lasers, and interband cascade lasers. He has authored or coauthored more than 50 scientific papers and more than ten granted patents in the fields of mid-infrared lasers and their applications.

Kevin Lascola received the M.S. degree in electrical engineering from the University of California, Berkeley, Berkeley, CA, USA, in 1997. Between 1997 and 2006, he was responsible for Product Engineering for multiple laser and photodetector products for SDL, Inc., and JDSU, including 980-nm pump lasers, source lasers, and high-speed avalanche photodiodes (APDs). Since 2007, he has been working on the development and production of quantum cascade lasers and interband cascade lasers for Maxion Technologies, Jessup, MD, USA, and Thorlabs, Newton, New Jersey, USA. In 2015, he became a Product Line Manager for mid-IR lasers at Thorlabs.

Steffen Becker received the B.Eng. degree in laser technology from the Aalen University of Applied Science, Aalen, Germany, in 2013, and the M.Sc. degree in photonics from the Friedrich-Schiller-University of Jena, Jena, Germany, in 2015. Also, in 2015, he joined the R&D division at Nanoplus Nanosystems and Technologies GmbH, where he is working on advanced sources for laser spectroscopy. His research interests are in the area of IR laser sources and their applications.

Lars Hildebrandt received the Ph.D. degree in physics in 2004 from the University of Potsdam, Potsdam, Germany, working with blue external cavity diode lasers for atom spectroscopy of indium and gas-sensing applications. He is the Director of sales with Nanoplus Nanosystems and Technologies GmbH, Gerbrunn, Germany, and has been working in the tunable semiconductor laser market since 1996, mainly in product development (external cavity diode laser and quantum cascade laser systems) and in sales and marketing. From 2005 to 2008, he was a Project Manager in the automotive industry for product innovation and introduction into series production. After gaining experience in this new business field, he started his focus toward semiconductor lasers in 2009. He is currently responsible for all sales and marketing activities for nanoplus.

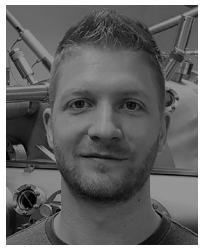

Robert Weih received the Diploma degree in physics of nanostructures and the Ph.D. degree in physics from Julius-Maximilians-University Wuerzburg, Wuerzburg, Germany, in 2011 and 2018, respectively. During his time at the Chair for Applied Physics, he was working on antimonide-based semiconductor devices for the mid-infrared spectral region. In 2015, he joined the Nanoplus Nanosystems and Technologies GmbH, where he is currently leading the Department of Chip Development and is continuing his research on the epitaxy and chip development of interband cascade lasers, interband cascade LEDs, and interband cascade detectors.

Alexey Belyanin received the Ph.D. degree in physics from the Russian Academy of Sciences, Moscow, Russia, in 1995. He is currently a Professor and the Associate Head of the Department of Physics and Astronomy, Texas A&M University, College Station, TX, USA. Prior to joining Texas A&M University, he was a Research Scientist with the Institute of Applied Physics of the Russian Academy of Sciences. His current research focuses on ultrafast, nonlinear, and quantum optics of semiconductor nanostructures and novel materials and the development of new optoelectronic devices. He has coauthored more than 140 papers in refereed journals and holds 5 patents, was the Chair of several international conferences, and was the recipient of a number of awards for research. He is a Fellow of the American Physical Society, Optical Society of America, and International Society for Optics and Photonics.

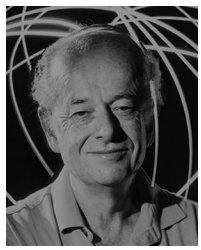

Federico Capasso is currently the Robert Wallace Professor of applied physics with Harvard University, Cambridge, MA, USA, which he joined in 2003 after 27 years at Bell Labs, where he rose from a Postdoctoral Researcher to the VP of Physical Research. He pioneered bandgap engineering of semiconductors, including the invention of the quantum cascade laser, and the field of flat optics with metasurfaces. He carried out high-precision measurements of the Casimir force with micro-electro-mechanical systems (MEMS) and the first measurement of the repulsive Casimir–Lifshitz force. He is a member of the National Academy of Sciences, the National Academy of Engineering, and the American Academy of Arts and Sciences. He was the recipient of the Fermi Prize of the Italian Physical Society, the Balzan Prize for Applied Photonics, the King Faisal Prize for Science, the IEEE Edison Medal, the APS Arthur Schawlow Prize, the OSA Wood Prize, the SPIE Gold Medal, the Rumford Prize of the American Academy of Arts and Sciences, the Franklin Institute Wetherill Medal, and the Materials Research Society Medal.